J. Appl. Comput. Mech., xx(x) (2026) 1-11
DOI: 10.22055/jacm.2026.48782.5492

ISSN: 2383-4536
jacm.scu.ac.ir

Shahid Chamran University of Ahvaz

Journal of Applied and Computational Mechanics

Research Paper

Interactions between Defects and Imperfect Interfaces Analyzing by a Fast Multiple BEM

Cong Li[1], Bin Hu[2], Yan Meng[1]

[1] School of Civil Engineering, Anhui Jianzhu University, Hefei, China
[2] School of Civil Engineering and Architecture, Anhui University of Science & Technology, Huainan, China

Received September 24 2025; Revised January 06 2026; Accepted for publication January 25 2026.
Corresponding author: C. Li (licong@ahjzu.edu.cn)

Abstract. Imperfect interfaces and pores significantly influence the fracture mechanics of the multiphase structure. In the present work, a fast multiple boundary element method is developed for analyzing the interactions between cracks, pores, and imperfect interfaces. A novel variable-order asymptotic element is employed to capture the stress singularity, while an imperfect interface model connects the different material phases. Numerical results demonstrate that the interfacial strength considerably affects both the stress intensity factors and propagation paths of cracks. Furthermore, the presence of random defects is shown to induce crack initiation and propagation.

Keywords: Imperfect interface, Stress intensity Factor, Crack propagation path, Multiphase structure, Fast multipole BEM.

1. Introduction

The interfacial phase plays a critical role in governing the fracture behaviors of composites. Initially, some scholars modeled the interfacial phase as an ideal perfect interface [1, 2]. However, this idealized assumption fails to account for ubiquitous interface imperfections, such as microdefects and weak bonding. A perfect interface can lead to significant stress concentration within a very narrow region, whereas an imperfect interface can create a stress transition zone. This zone allows stress and elastic modulus to change smoothly from one material to another to avoid sharp stress peaks. Owing to this beneficial mechanism, the imperfect interfaces have been successfully applied in various engineering fields, such as thermal conductivity [3-6], multiferroic nanofibrous composites [7-9], PN junction [10, 11], spherical–circular inclusion composites [12-15], etc., they all obtain satisfactory results.

Imperfect interfaces are commonly modeled using the viscoelastic model [16], the rigid model [17], or the spring model [18, 19]. The influence of imperfect interfaces on fracture response has been investigated using various numerical methods, including the finite element method (FEM) [20, 21], boundary element method (BEM) [22], and phase-field method [23, 24], etc. For instance, Yang et al. [20] combined FEM and virtual crack closure technique (VCCT) to analyze cracks-oriented perpendicular to imperfect interfaces. Stankevych [22] employed BEM to study interfacial behavior under various contact conditions, ranging from perfect bonding to thin compliant interlayers. Zambrano et al. [23] integrated the phase-field method with cohesive zone elements to examine how the phase-field continuity affects crack kinking at interfaces.

In this work, we aim at investigating interactions between defects and imperfect interfaces using the fast multipole boundary element method (FMBEM). Unlike previous works, where the crack is typically located at the interface, the crack in this study is situated near the imperfect interface. To accurately capture the stress singularities at the crack tip, a novel variable-order asymptotic element (VAE) is implemented in the vicinity of the tip. Furthermore, four kinds of imperfect interface models are integrated into an advanced FMBEM to compute the complete stress and displacement fields, as well as the fracture responses of multiphase structures with an imperfect interface.

2. Boundary Integral Equations for a Bi-material Cracked Structure

Consider a 2D elastic cracked structure, as seen in Fig. 1. The conventional boundary integral equation (CBIE) and the hyper-singular boundary integral equation (HBIE) [25] can be written as follows:

$$c_{ij}(\mathbf{y})u_j(\mathbf{y}) = \int_\Gamma U^*_{ij}(\mathbf{x},\mathbf{y})t_j(\mathbf{y})\,\mathrm{d}\Gamma - \int_\Gamma T^*_{ij}(\mathbf{x},\mathbf{y})u_j(\mathbf{y})\,\mathrm{d}\Gamma, \qquad \mathbf{y}\in\Gamma,\ \ \mathbf{x}\in\Gamma \tag{1}$$

$$c_{ij}(\mathbf{y})t_j(\mathbf{y}) = \int_\Gamma K^*_{ijk}(\mathbf{x},\mathbf{y})t_j(\mathbf{y})\,\mathrm{d}\Gamma - \int_\Gamma H^*_{ijk}(\mathbf{x},\mathbf{y})u_j(\mathbf{y})\,\mathrm{d}\Gamma, \qquad \mathbf{y}\in\Gamma_c,\ \ \mathbf{x}\in\Gamma \tag{2}$$

Published online: February 17 2026

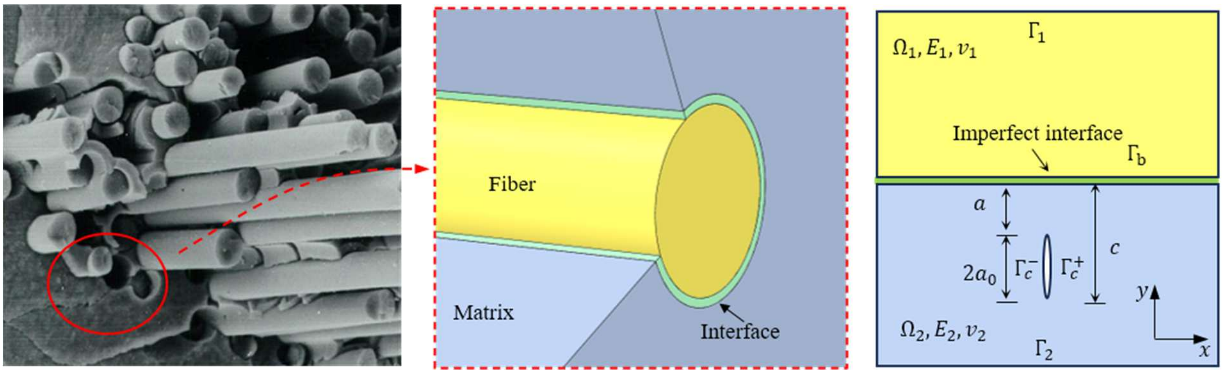

Fig. 1. A bi-material cracked structure with an imperfect interface.

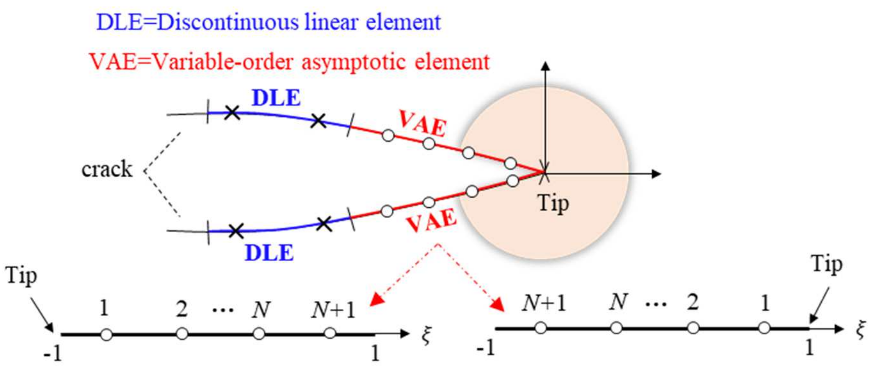

Fig. 2. A novel variable-order asymptotic element.

where $\mathbf{x}$ is the field point and $\mathbf{y}$ is the source point. $u_j(\mathbf{x})$ and $t_j(\mathbf{x})$ are the displacements and tractions at $\mathbf{x}$, respectively. $c_{ij}(\mathbf{y})$ is a coefficient. $U^*_{ij}(\mathbf{x},\mathbf{y})$, $T^*_{ij}(\mathbf{x},\mathbf{y})$, $K^*_{ijk}(\mathbf{x},\mathbf{y})$ and $H^*_{ijk}(\mathbf{x},\mathbf{y})$ are the fundamental solutions for plane strain cases:

$$U^*_{ij}(\mathbf{x},\mathbf{y}) = \frac{1}{8\pi\mu(1-\nu)}[(3-\nu)\delta_{ij}\ln\frac{1}{r} + r_{,i}r_{,j} - \frac{1}{2}\delta_{ij}] \tag{3}$$

$$T^*_{ij}(\mathbf{x},\mathbf{y}) = \frac{-1}{4\pi(1-\nu)r}\{[(1-2\nu)\delta_{ij} + 2r_{,i}r_{,j}]\frac{\partial r}{\partial n} - (1-2\nu)(r_{,i}n_j - r_{,j}n_i)\} \tag{4}$$

$$K^*_{ijk}(\mathbf{x},\mathbf{y}) = \frac{1}{4\pi(1-\nu)r}[(1-2\nu)(\delta_{ij}r_{,k} + \delta_{jk}r_{,i} - \delta_{ik}r_{,j}) + 2r_{,i}r_{,j}r_{,k}]n_k \tag{5}$$

$$H^*_{ijk}(\mathbf{x},\mathbf{y}) = \frac{\mu}{2\pi(1-\nu)r^2}\{2r_{,n}[(1-2\nu)\delta_{ik}r_{,j} + \nu(\delta_{ij}r_{,k} + \delta_{jk}r_{,i}) - 4r_{,i}r_{,j}r_{,k}] + 2\nu(n_ir_{,j}r_{,k} + n_kr_{,i}r_{,j}) - (1-4\nu)n_j\delta_{ik} + (1-2\nu)(2n_jr_{,i}r_{,k} + n_k\delta_{ij} + n_i\delta_{jk})\}n_k \tag{6}$$

where $(\cdots)_{,i} = \partial(\cdots)/\partial x_i$, n_i is the outward normal vector. r is the distance between $\mathbf{x}$ and $\mathbf{y}$. E and ν are Young's modulus and Poisson's ratio, respectively, and $\mu = E/[2(1+\nu)]$. For plane stress problems, ν is replaced with $\nu/(1+\nu)$.

If the crack belongs to a single domain, Both CBIE and HBIE are established on the crack surfaces to avoid the ill-posedness of the system equation. If the crack is at the interface, only CBIE is required.

3. A Novel Variable-order Asymptotic Element

As we all know, the stresses near the V-notch /crack tip region are singular, the traditional BEM cannot capture the accurate singular stress fields. A novel variable-order asymptotic element (VAE) [26-28] is first used in the defect tip in the present study:

$$\begin{cases} u_i = \sum_{k=1}^{N}(\frac{1+\vartheta\xi}{2})^{d_k}\tilde{u}_i^{(k)} - \frac{1+\vartheta\xi}{2}\sum_{k=1}^{N}\tilde{u}_i^{(k)} + \frac{1+\vartheta\xi}{2}u_i^{N+1} \\ t_i = \sum_{k=1}^{N}(\frac{1+\vartheta\xi}{2})^{s_k}\tilde{t}_i^{(k)} - \frac{1+\vartheta\xi}{2}\sum_{k=1}^{N}\tilde{t}_i^{(k)} + \frac{1+\vartheta\xi}{2}t_i^{N+1} \end{cases}, \quad \text{i=1,2} \tag{7}$$

where d_k and s_k are the displacement and stress exponents, respectively. The d_k and s_k are obtained by the interpolation matrix method proposed by Niu [29]. $\tilde{u}_i^{(k)}$ and $\tilde{t}_i^{(k)}$ are the displacement and traction coefficients, respectively. If the V-notch/crack tip is at $\xi = -1.0$, $\vartheta = 1.0$. If the V-notch/crack tip is at $\xi = 1.0$, $\vartheta = -1.0$. u_i^{N+1} and t_i^{N+1} are the displacement and traction at the other end of the VAE away from the tip, respectively. These features enable the VAE to be connected directly to the conventional elements without the connective elements. By using the VAE in the defect tip, the singular stress fields near the tip region can be obtained accurately.

4. Linear Spring Model for an Imperfect Interface

For the interfacial layer between Ω_1 and Ω_2 (see Fig. 1), the linear spring model is used [30], where the relationship between tractions and displacements on the imperfect interface is as follows:

$$t_x^1 = -t_x^2 = \beta_x(u_x^1 - u_x^2) \tag{8}$$

$$t_y^1 = -t_y^2 = \beta_y(u_y^1 - u_y^2) \tag{9}$$

where *t* and *u* are the tractions and displacements, respectively. β_x, β_y are interface parameters that do not affect each other. The superscript 1 and 2 represent the physical quantities corresponding to Ω_1 and Ω_2, respectively.

From Eqs. (8-9), we can know that, if $\beta_x \to 0$ and $\beta_y \to 0$, the interface is a separate interface (SEI). If $\beta_x \to \infty$ and $\beta_y \to \infty$, the interface is a perfect interface (PEI). If $\beta_x \to 0$ and $\beta_y \to \infty$, the interface is a sliding interface (SLI). If $\beta_x \to \infty$ and $\beta_y \to 0$, the interface is a winkler interface (WII). SEI and PEI are special cases of the linear spring model.

5. FMBEM Analysis for the Cracked Structure with Imperfect Interfaces

Different a single-phase structure without defects, the system equations established by the FMBEM is more complicate. For the general boundary, only two quantities (displacements or tractions) for a node are unknown, but there are four unknowns for one node at both the crack surface and the interface. Taking the structure of Fig. 1 as an example, the number of nodes on Γ_1 and Γ_b are *M* and *Q*, respectively, the number of unknowns is 2*M* + 4*Q* in Ω_1. The number of nodes on Γ_2 and Γ_c are *L* and *P*, respectively, the number of unknowns is 2*L* + 4*P* + 4*Q* in Ω_2. Because Γ_b is the interface of Ω_1 and Ω_2, the tractions are the linear function of the displacements, as shown in Eqs. (8-9), so the unknowns of Ω_1 and Ω_2 are 2*M* + 2*L* + 4*P* + 4*Q* in total. Note that crack is in the Ω_2, 2*Q* CBIEs (1) are established in Γ_c^+, and 2*Q* HBIEs (2) are established in Γ_c^-. Consequently, the matrix equation is as follows:

$$\begin{bmatrix} \mathbf{T}_{11} & \mathbf{T}_{12}^{B} & 0 & 0 & 0 \\ \mathbf{T}_{121}^{B} & \mathbf{T}_{1212}^{B\,B} & 0 & 0 & \mathbf{T}_{122}^{B} \\ 0 & \mathbf{T}_{c112}^{+\,B} & \mathbf{T}_{c1c1}^{+\,+} & \mathbf{T}_{c1c1}^{+\,-} & \mathbf{T}_{c22}^{-} \\ 0 & \mathbf{H}_{c112}^{-\,B} & \mathbf{H}_{c1c1}^{-\,+} & \mathbf{H}_{c1c1}^{-\,-} & \mathbf{H}_{c22}^{-} \\ 0 & 0 & 0 & \mathbf{T}_{221}^{B} & \mathbf{T}_{22} \end{bmatrix} \begin{bmatrix} \mathbf{u}_1 \\ \mathbf{u}_{12}^{B} \\ \mathbf{u}_{c1}^{+} \\ \mathbf{u}_{c1}^{-} \\ \mathbf{u}_2 \end{bmatrix} = \begin{bmatrix} \mathbf{U}_{11} & \mathbf{U}_{12}^{B} & 0 & 0 & 0 \\ \mathbf{U}_{121}^{B} & \mathbf{U}_{1212}^{B\,B} & 0 & 0 & \mathbf{U}_{122}^{B} \\ 0 & \mathbf{U}_{c112}^{+\,B} & \mathbf{U}_{c1c1}^{+\,+} & \mathbf{U}_{c1c1}^{+\,-} & \mathbf{T}_{c22}^{-} \\ 0 & \mathbf{K}_{c112}^{-\,B} & \mathbf{K}_{c1c1}^{-\,+} & \mathbf{K}_{c1c1}^{-\,-} & \mathbf{K}_{c22}^{-} \\ 0 & 0 & 0 & \mathbf{U}_{221}^{B} & \mathbf{U}_{22} \end{bmatrix} \begin{bmatrix} \mathbf{t}_1 \\ \mathbf{t}_{12}^{B} \\ \mathbf{t}_{c1}^{+} \\ \mathbf{t}_{c1}^{-} \\ \mathbf{t}_2 \end{bmatrix} \tag{10}$$

where $\mathbf{u}_1$, $\mathbf{t}_1$ are unknown displacements and tractions on Γ_1 respectively, 2*M* in total. $\mathbf{u}_2$, $\mathbf{t}_2$ are unknown displacement and traction on Γ_2 respectively, 2*L* in total. $\mathbf{u}_{12}^B$, $\mathbf{t}_{12}^B$ are unknown displacement and traction on Γ_b respectively, 4*Q* in total. $\mathbf{u}_{c1}^+$, $\mathbf{t}_{c1}^+$ are unknown displacement and traction on Γ_c^+ respectively, 2*P* in total. $\mathbf{u}_{c1}^-$, $\mathbf{t}_{c1}^-$ are unknown displacement and traction on Γ_c^- respectively, 2*P* in total. ***T***, ***U*** are the coefficient matrix of CBIE (Eq. (1)) with respect to displacement and traction. ***H***, ***K*** are the coefficient matrix of HBIE (Eq. (2)) with respect to displacement and traction. Hence, all unknown boundary displacements and tractions of the cracked structure with an imperfect interface are obtained by solving Eq. (10).

After the whole displacement and stress fields are obtained, the displacement extrapolation method and the maximum circumferential stress criterion are used to obtain the crack propagation path. Firstly, the crack-tip opening displacement method (CTOD) is used to calculate the stress intensity factors K_{I} and K_{II}:

$$K_{\mathrm{I}} = \lim_{r \to 0} \sqrt{2\pi} \frac{\mu}{1+\kappa} \frac{\Delta u_n}{\sqrt{r}} \tag{11}$$

$$K_{\mathrm{II}} = \lim_{r \to 0} \sqrt{2\pi} \frac{\mu}{1+\kappa} \frac{\Delta u_\tau}{\sqrt{r}} \tag{12}$$

where $\kappa = 3 - 4\nu$ for plane strain, $\kappa = (3-\nu)/(1+\nu)$ for plane stress. Δu_τ, Δu_n is the relative displacement of two crack surface along τ and *n* respectively, as seen in Fig. 3.

Then, based on the maximum circumferential stress criterion, the crack initiation angle θ can be determined by:

$$K_{\mathrm{I}} \sin\theta + K_{\mathrm{II}}(3\cos\theta - 1) = 0 \tag{13}$$

$$\theta = 2\arctan\left(\frac{K_{\mathrm{I}} - \sqrt{K_{\mathrm{I}}^2 + 8K_{\mathrm{II}}^2}}{4K_{\mathrm{II}}}\right) \tag{14}$$

Finally, the effective stress intensity factor K_{eff} of each crack tip is obtained by:

$$K_{\mathrm{eff}} = K_{\mathrm{I}} \cos^3\left(\frac{\theta}{2}\right) - 3K_{\mathrm{II}} \cos^2\left(\frac{\theta}{2}\right) \sin\left(\frac{\theta}{2}\right) \tag{15}$$

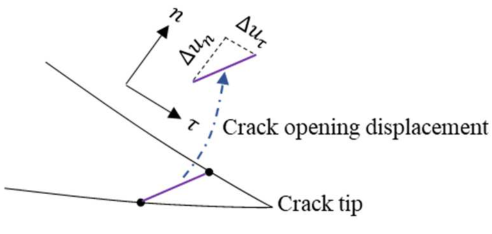

Fig. 3. Crack opening displacement.

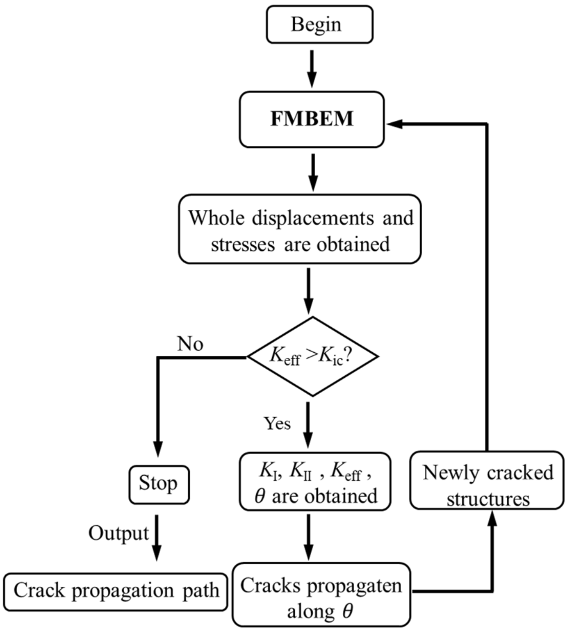

Fig. 4. The flowchart of FMBEM implementation process.

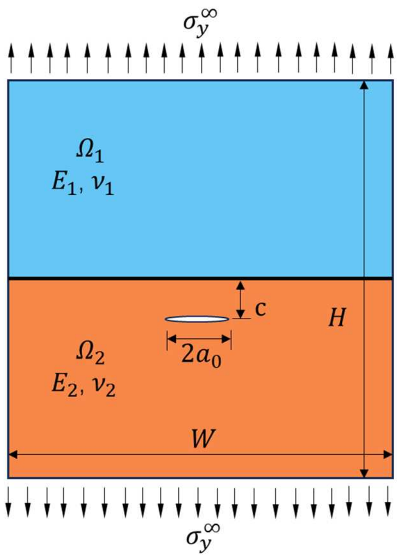

Fig. 5. A bi-material plate with a single crack and an imperfect interface.

If the K_{eff} is larger than the material toughness K_{IC}, the crack propagates forward along the direction of the θ to form a new multi-cracked structure. Note that the crack doesn't propagate when $K_{eff} < K_{IC}$. The flowchart of FMBEM can be seen in Fig. 4.

6. Numerical Examples

6.1. The interaction between a single crack and an imperfect interface

A bi-material plate with a single crack and an imperfect interface under tension is considered, as shown in Fig. 5. The width and height of the plate W × H = 20 mm × 20 mm. There is a crack parallel to the interface in Ω_2, the length of the crack is a_0 and the distance from the crack to the interface is c, where c is variable. E_1 and E_2 are Young's modulus of Ω_1 and Ω_2, respectively. ν_1 and ν_2 are Poisson's ratio of Ω_1 and Ω_2, respectively, σ_y^∞ = 100 MPa.

A simple benchmark case is first considered to verify the accuracy of the present method. Let $E_1 = E_2 = 100$GPa, c = 1 mm, the stress intensity factor K_I with PEI under different a_0 / c are discussed, as shown in Table 1.

Table 1. Stress intensity factor K_I (MPa$\sqrt{\text{m}}$).

a_0/c	0.1	0.2	0.3	0.4	0.5	0.6
FMBEM	127.13	179.95	227.74	276.25	330.36	396.53
Analytic solution [31]	126.08	181.58	229.57	278.00	332.44	399.94
Relative error	0.8%	0.9%	0.8%	0.6%	0.6%	0.9%

It can be observed from Table 1 that, the relative error ([FMBEM-Analytic solution]/FMBEM · 100%) of stress intensity factor K_I are all less than 1%, which shows the FMBEM can obtain the stress intensity factor accurately.

Next, a composite structure with aluminum and steel is analyzed. The Young's moduli of aluminum and steel are 80.0 and 208 GPa, respectively. The Poisson's ratios are 0.33 and 0.3, respectively. From Fig. 6, we can see that K_I increase with the increase of a_0/c, indicating a greater fracture risk as the crack propagates toward the interface. The smallest K_I value is observed for the crack with PEI, while the largest occurs with SEI. These results demonstrate that the interfacial strength significantly influences the safety of the multiphase structure.

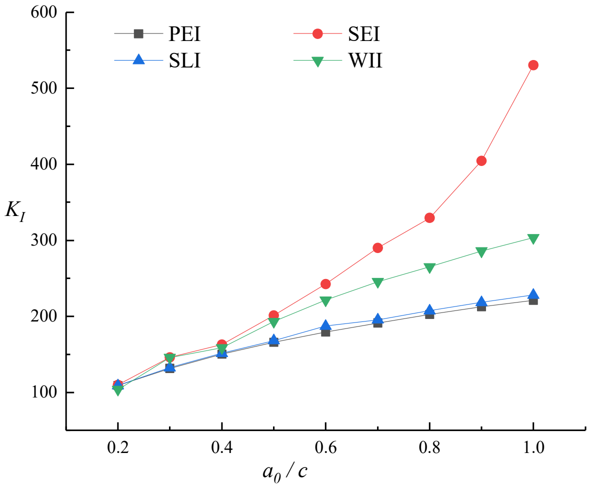

Fig. 6. Stress intensity factor K_I under different a_0/c (MPa$\sqrt{m}$).

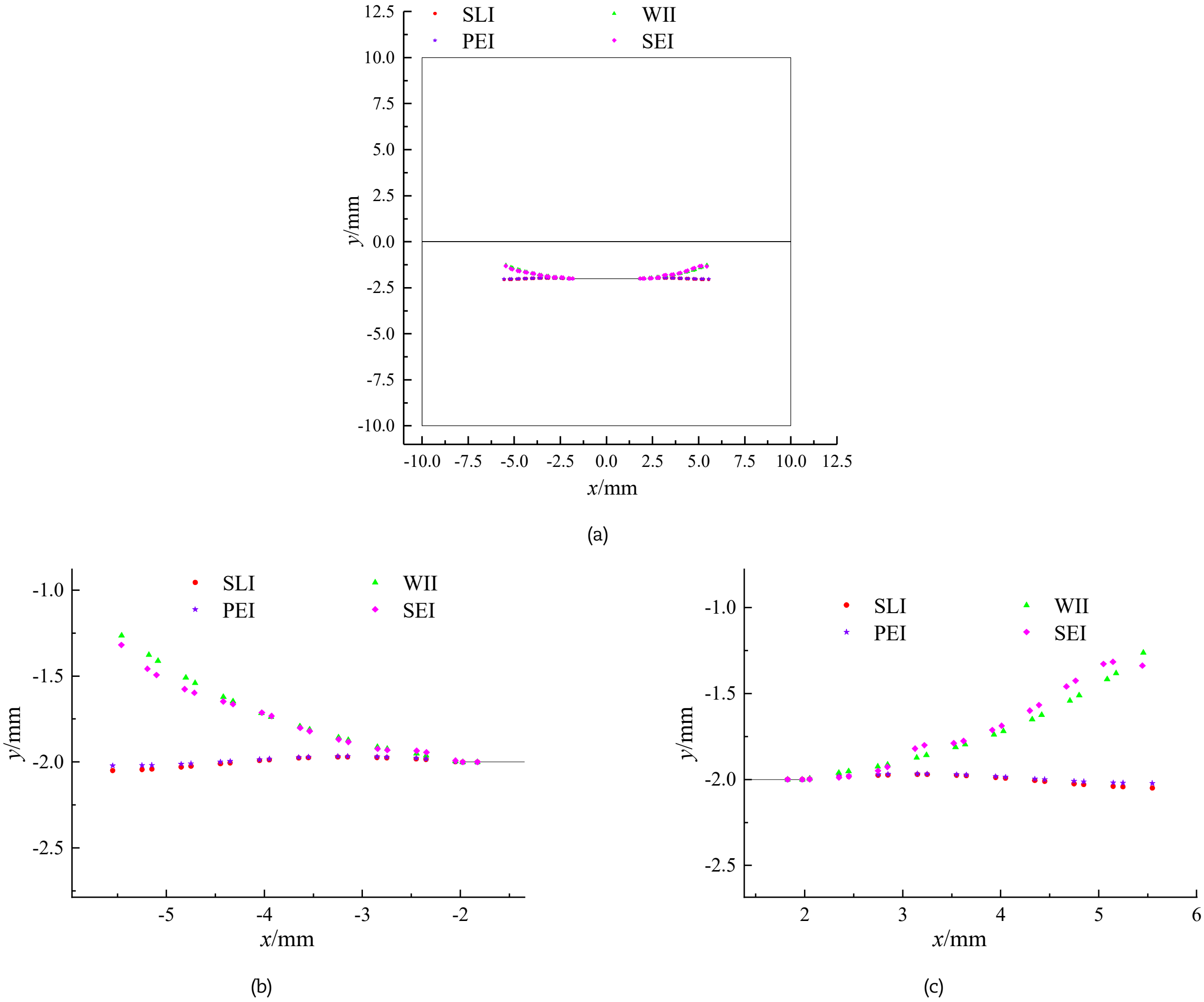

Fig. 7. Crack propagation paths after 10 increment steps when a_0/c = 1, (a) Crack propagation path, (b) Enlarged view of the left crack tip, (c) Enlarged view of the right crack tip.

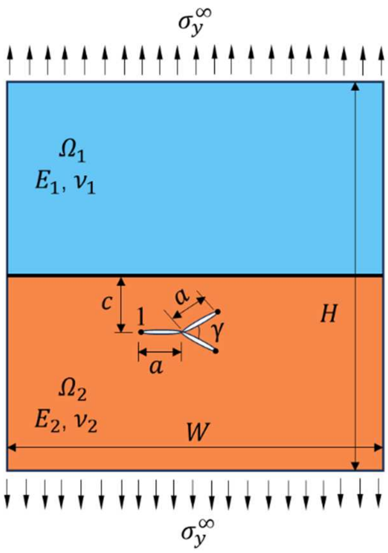

Fig. 8. A plate with a branch crack and an imperfect interface.

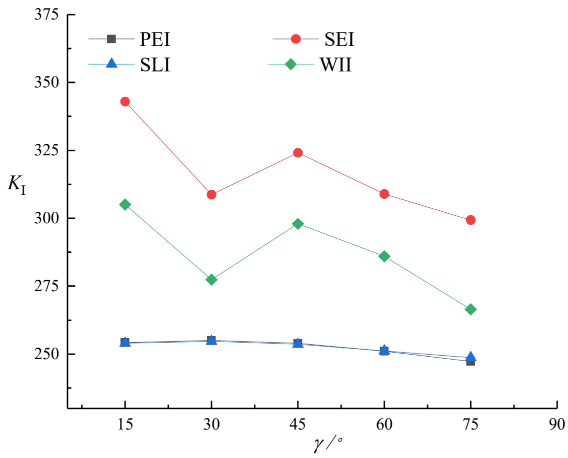

Fig. 9. The stress intensity factor K_I for different angle γ (MPa$\sqrt{m}$).

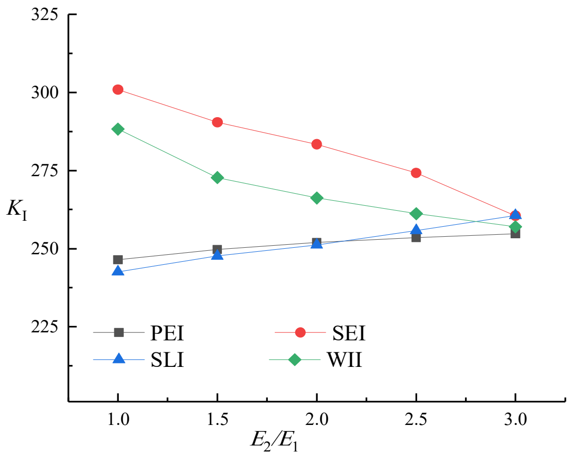

Fig. 10. The stress intensity factors K_I for different E_2 / E_1(MPa$\sqrt{m}$).

Figure 7(a) shows the whole crack propagation paths for the multiphase structure with different interfaces. Figures 7(b) and 7(c) are the enlarged view of left and right part, respectively. For the structures with SLI and PEI, the Mode I crack continues to extend along its original path. In contrast, for structures with SEI and WII, the crack path deviates toward the interface. The video of crack propagation path can be seen in https://www.researchgate.net/publication/399443553_The_Video_of_Crack_propagation_path.

6.2. The interaction between a branch crack and an imperfect interface

A bi-material plate with a branch crack and an imperfect interface under tension is considered, as shown in Fig. 8. The length of the crack branch is a = 2 mm, the angle between two branches is γ. The width and height of the plate W × H = 20 mm × 20 mm. $\nu_1 = \nu_2 = 0.25$, $\sigma_y^\infty = 100\text{MPa}$. E_1 and E_2 are Young's modulus of Ω_1 and Ω_2, respectively.

Figure 9 shows the variation of stress intensity factor K_I at Node 1 for different angle γ when $E_2/E_1 = 2$. For structures with SLI and PEI, K_I exhibits minimal sensitivity to the change in γ. In contrast, for structures with SEI and WII, K_I shows a pronounced dependence on the angle.

The values of the stress intensity factor K_I at Node 1 for different Young's modulus ratios E_2/E_1 at $\gamma = 60^\circ$ are calculated and shown in Fig. 10. For the structure with SEI and WII, K_I decreases with the increase of E_2/E_1. Conversely, for the structure with SLI and PEI, K_I increases with the increase of E_2/E_1. Notably, the K_I values for all four cases converge to a similar value when E_2/E_1, indicating that the influence of the interface diminishes as the stiffness of Ω_2 increases significantly relative to Ω_1.

6.3. The interaction among an imperfect interface, multiple cracks and pores

A bi-material plate with an imperfect interface, multiple cracks and pores under tension is considered, as shown in Fig. 11. The width and height of the plate W × H = 200 mm × 200 mm. E_1 = 50 GPa, E_2 = 100 GPa, $\nu_1 = \nu_2 = 0.25$, $\sigma_y^\infty = 100$ MPa.

Figure 12 shows the crack propagation paths of the structure with PEI, SLI, SEI and WII. The results indicate that the cracks in a plate with PEI (Fig. 12(a)) propagate slower than those in a plate with imperfect interface (Figs. 12(b), (c), (d)). Among the imperfect interfaces, the SEI exhibits the most significant effect in promoting crack initiation and propagation.

Next, a bi-material plate with multiple cracks, pores, and an imperfect interface is analyzed, as shown in Fig. 11(b). The corresponding crack propagation paths after 20 increment steps is presented in Fig. 13. A comparison between Figs. 12 and 13 reveals that the presence of random pores accelerates and extends crack propagation. These pores serve as stress concentrators, thereby weakening the structural strength. If the multi-cracked structure has both random pores and imperfect interfaces, the crack propagation is further accelerated.

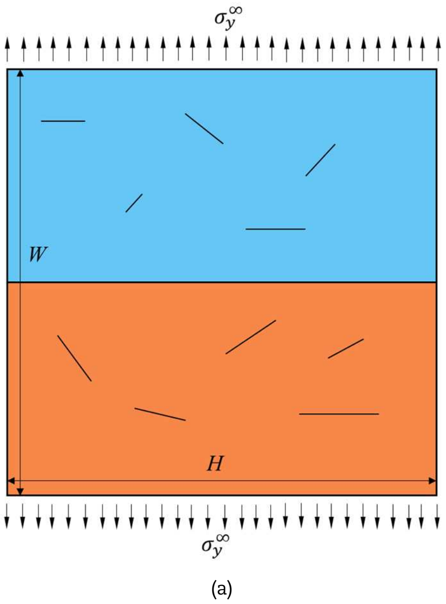

Fig. 11. A plate with multi-cracks and an imperfect interface, (a) No pores, (b) Random pores.

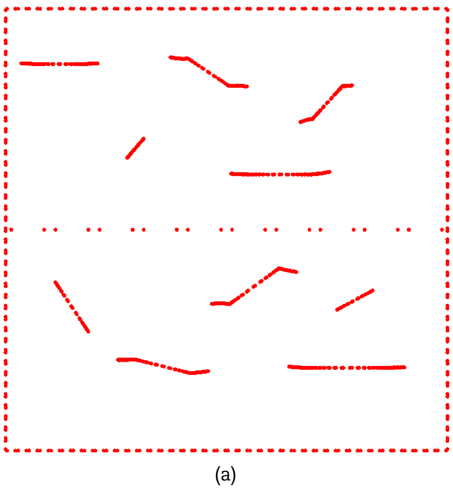

Fig. 12. The crack propagation paths of the structure, (a) PEI, (b) SEI, (c) SLI, (d) WII.

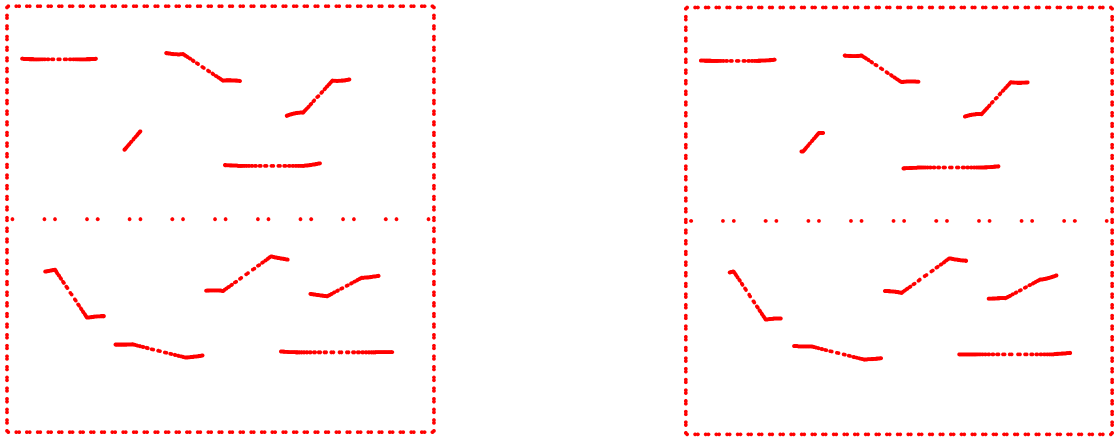

(c) (d)

Fig. 12. Continued.

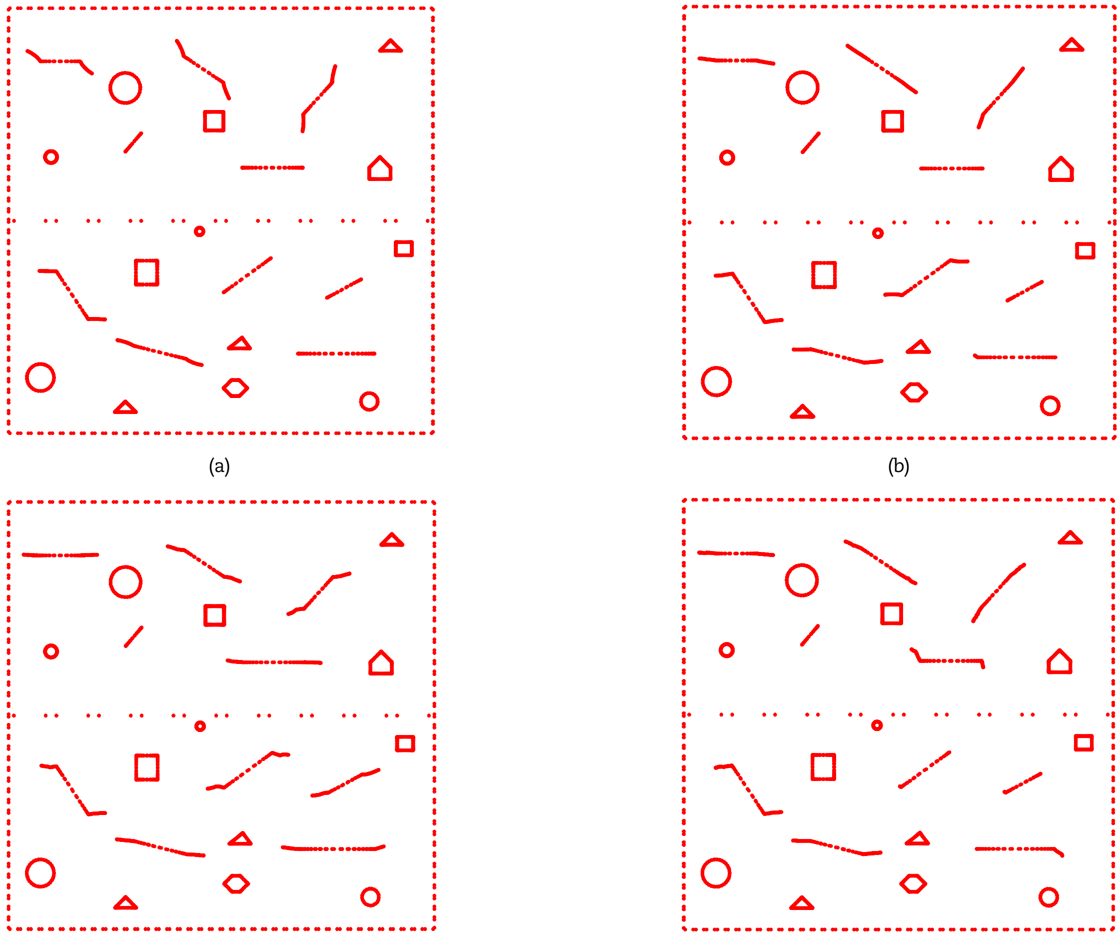

(a) (b) (c) (d)

Fig. 13. The crack propagation path of the structure with random pores, (a) PEI, (b) SEI, (c) SLI, (d) WII.

Finally, a bi-material plate (200 mm × 200 mm) containing 400, 800, 1200, 1600, 2000 cracks under an imperfect interface is studied, as illustrated in Fig. 14. The Young's modulus of two phases are 50 GPa and 100 GPa, respectively. The Poisson's ratios of two phases are both 0.25. The model is subjected to a tensile stress of 100 MPa. The computations are done on a AMD Ryzen 7 6800H laptop with a 3.20 GHz CPU. Table 2 shows that the number of degrees of freedom (DOFs) and CPU time for a plate with varying number of cracks. With the increase of the number of DOFs, the computational time grows very slowly, demonstrating the high computational efficiency of the proposed method.

Table 2. The degree of freedom and evaluation time used in present method.

The number of cracks	400	800	1200	1600	2000
DOFs	15768	29360	43976	57976	72784
CPU time(sec)	246	297	371	578	814

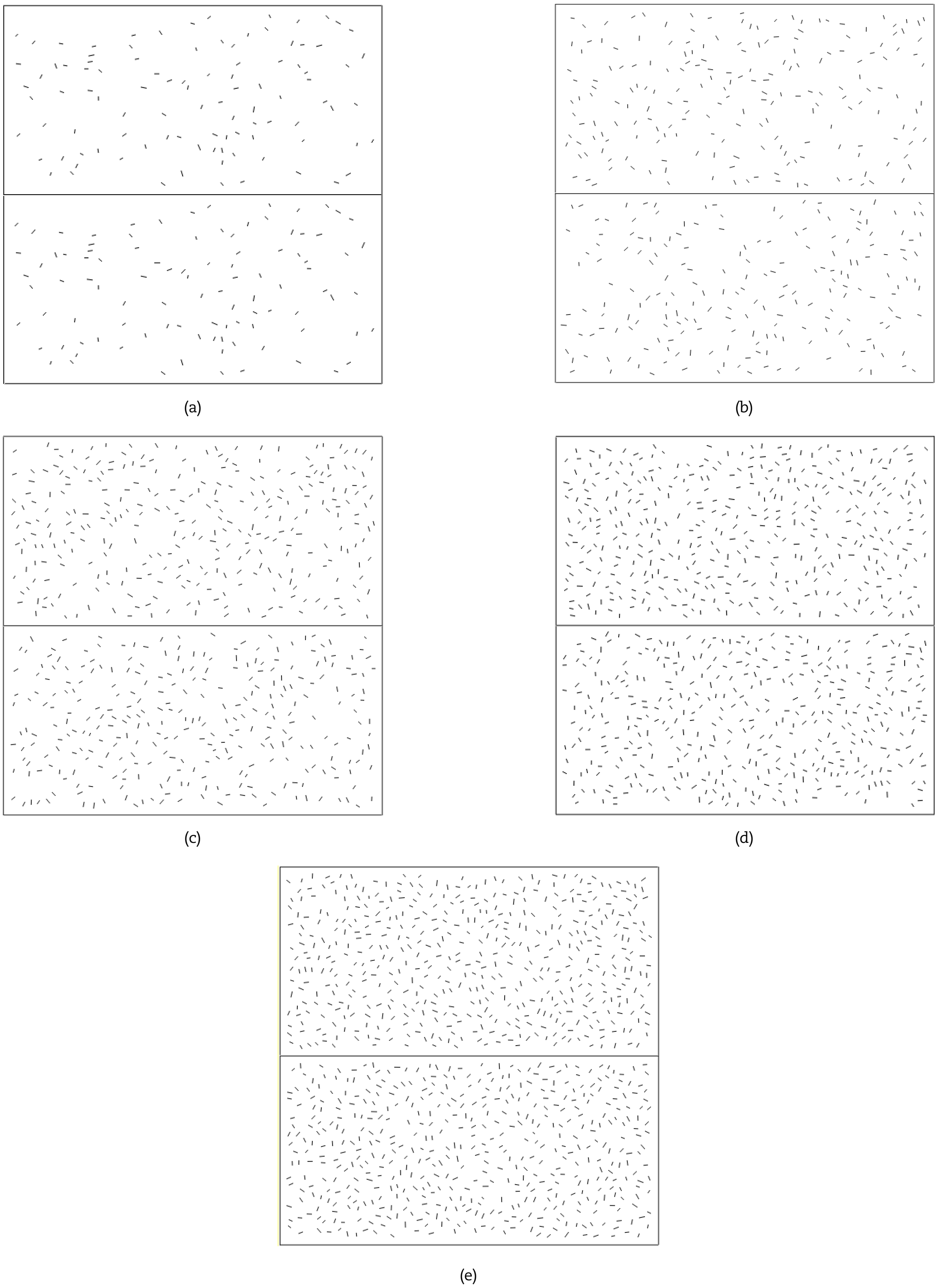

Fig. 14. A plate with multi-cracks and an imperfect interface, (a) 400 cracks, (b) 800 cracks, (c) 1200 cracks, (d) 1600 cracks, (e) 2000 cracks.

7. Conclusions

A fast multipole boundary element method with VAEs is first used to study the interactions between cracks, pores, and imperfect interfaces modeled by the linear spring model. Some interesting phenomena are revealed.

(1) The structure is at greater risk when a crack is located near a weak interface. In structures with SLI or PEI, the Mode I crack tends to propagate straight along its original path. In contrast, for structures featuring SEI or WII, the crack deflects toward the interface.

(2) For the cracked structure with SLI and PEI, the branch angle has little impact on the stress intensity factor. In contrast, for the cracked structure with SEI and WII, the branch angle significantly influences the stress intensity factor.
(3) The presence of random pores and an imperfect interface can weaken the strength of the structure and induce crack initiation.

Author Contributions

C. Li planned the scheme, initiated the project; B. Hu developed the mathematical modeling and examined the theory validation; Y. Meng examined the theory validation. The manuscript was written through the contribution of all authors. All authors discussed the results, reviewed, and approved the final version of the manuscript.

Acknowledgments

Not applicable.

Conflict of Interest

The authors declared no potential conflicts of interest concerning the research, authorship, and publication of this article.

Funding

This work was supported by the Natural Science Research Project of the Anhui Educational Committee [No. 2024AH030010], the National Natural Science Foundation of China [No. 12202001], and Domestic Visiting Scholar Project of Anhui Educational Committee [No. JNFX2024027].

Data Availability Statements

The datasets generated and/or analyzed during the current study are available from the corresponding author on reasonable request.

References

[1] Li, X.F., Fan, T.Y., The asymptotic stress field for a rigid circular inclusion at the interface of two bonded dissimilar elastic half space materials, *International Journal of Solids and Structures*, 38, 2001, 44-45.
[2] Shin, K.C., Liu, H., Lee, J.J., Choi, S.T., Interfacial crack tip field in anisotropic isotropic biomaterials, *Composite Structures*, 66, 2004, 1-4.
[3] Ahamed, A.N., Pandi, Pitchai, P.J., Guruprasad., Determination of the effective thermal conductivity of composites under the influence of an imperfect interface using a variational asymptotic-based method, *Archive of Applied Mechanics*, 94, 2024, 3597-3624.
[4] Benveniste, Y., Miloh, T., The effective conductivity of composites with imperfect thermal contact at constituent interfaces, *International Journal of Engineering Science*, 24(9), 1986, 1537-1552.
[5] Lequang, H., Phan, T.L., Bonnet, G., Effective thermal conductivity of periodic composite switch highly conducting imperfect interfaces, *International Journal of Thermal Sciences*, 50(8), 2011, 1428-1444.
[6] Nguyen, D.H., Le, Q.H., He, Q.C., Tran A.T., Generalized hill-mendel lemma and equivalent inclusion method for determining the effective thermal conductivity of composites with imperfect interfaces, *Applied Mathematical Modelling*, 90, 2021, 624-649.
[7] Chang, L.H., Cheng, S.M., Zhang, J.S., Wang W.S., Effective magneto-electro-elastic moduli for multiferroic nanofibrous composites with imperfect interface, *Acta Mechanica*, 236, 2025, 563-584.
[8] Chen, Y., Guo, J., Effective property of piezoelectric composites containing coated nano-elliptical fibers with interfacial debonding, *Applied Mathematics and Mechanics*, 43(11), 2022, 1701-1716.
[9] Almeyd, Y.E., Montes, H.C., Ramos, R.R., Guinovart-díaz, R., López-realppozo, J.C., Bravo-Castillero, J., Sabina, F.J., Influence of imperfect interface and fiber distribution on the antiplane effective magneto-electro-elastic properties for fiber reinforced composites, *International Journal of Solids and Structures*, 112, 2017, 155-168.
[10] Wei, Z.B., Wei, P.J., Xu, C.Y., Guo, X., Equivalent imperfect interface model of PN junction of piezoelectric semiconductor for the multi-field coupled waves propagation, *Acta Mechanica*, 235, 2024, 73-92.
[11] Loukkal, A., Lematre, M., Bavencoffe, M., Lethiecq, M., Modeling and numerical study of the influence of imperfect interface properties on the reflection coefficient for isotropic multilayered structures, *Ultrasonics*, 103, 2020, 106099.
[12] Duc-Chinh, P., Trung-Kien, N., General imperfect interface model for spherical–circular inclusion composites, *Acta Mechanica*, 235, 2024, 2211-2229.
[13] Zhang, Q.Q., Zhang, R.F., Li, H.Y., Zhang, L.J., Wang, S., Gao, C.F., Thermal-elastic field around an elliptical nano-inclusion with interface conduction and interface stress effects, *Acta Mechanica*, 234, 2023, 6395-6406.
[14] Levin, V., Markov, M., Effective thermal conductivity of micro-inhomogeneous media containing imperfectly bonded ellipt social inclusions, *International Journal of Engineering Science*, 109, 2016, 202-215.
[15] Bonfoh, N., Sabar, H., Anisotropic thermal conductivity of composites with ellipsoidal inclusions and highly conducting interfaces, *International Journal of Heat and Mass Transfer*, 118, 2018, 498-509.
[16] Wang, X., Pan, E., Chung, P.W., Some basic problems in anisotropic bimaterials with a viscoelastic interface, *International Journal of Solids and Structures*, 46(20), 2009, 3725-373.
[17] Benveniste, Y., Miloh, T., Imperfect soft and stiff interfaces in two-dimensional elasticity, *Mechanics of Materials*, 33(6), 2001, 309-323.
[18] Chen, W.Q., Zhou, Y.Y., Lu, C.F., Ding, H.J., Bending of multiferroic laminated rectangular plates with imperfect interlaminar bonding, *European Journal of Mechanics A/Solids*, 28(4), 2009, 720-727.
[19] Zhong, X.C., Li, X.F., Lee, K.Y., Analysis of a mode-I crack perpendicular to an imperfect interface, *International Journal of Solids and Structures*, 46(6), 2009, 1456-1463.
[20] Yang, H.Q., Wang, R.H., Zhou, W.D., Fracture analysis of crack perpendicular to an imperfect bimaterial interface, *Science Technology and Engineering*, 13(35), 2013, 10450-10454. (in Chinese)
[21] Nairn, J.A., Numerical implementation of imperfect interfaces, *Computational Materials Science*, 40, 2007, 525-536.
[22] Stankevych, V.Z., Stankevych, O.M., Acoustic emission in elastic bimaterial with crack under different contact conditions on interface plane, *International Applied Mechanics*, 60, 2024, 203-211.

[23] Zambrano, ToroS, Sánchez, P., Duda, F.P., Méndez C.G., Huespe A.E., Interaction analysis between a propagating crack and an interface: Phase field and cohesive surface models, *International Journal of Plasticity*, 156, 2022, 103341.
[24] Salman, K., Chandrasekhar, A., Antonio, R.F., Investigation on the effect of material mismatch between two dissimilar materials using an adaptive phase-field method, *International Journal of Advanced in Engineering Scienced and Applied Mathematics*, 15, 2023, 173-186.
[25] Liu, Y.J., *Fast multipole boundary element method*, Cambridge University Press, 2009.
[26] Li, C., Hu, B., Niu, Z.R., Meng, Y., An advanced fast multipole dual boundary element method for analyzing multiple cracks propagation, *Engineering Fracture Mechanics*, 311, 2024, 110547.
[27] Hu, B., Niu, Z. R., Li, C., Hu, Z.J., A fast multipole boundary element method based on higher order elements for analyzing 2-D elastostatic problems, *Engineering Analysis with Boundary Elements*, 130(2), 2021, 417-428.
[28] Li, C., Meng, Y., Hu, B., Niu, Z.R., Estimation of stress intensity factor by using a new fast multipole dual-boundary element method, *Mathematics*, 13, 2025, 842.
[29] Niu, Z.R., Li, C., Cheng, C.Z., Hu, B., *Interpolation matrix method for ordinary differential equations and its mechanical applications*, University of Science and Technology of China Press, Anhui, 2023. (in Chinese)
[30] Benveniste, Y., The effective mechanical behavior of composite materials with imperfect contact between the constituents, *Mechanics of Materials*, 4(2), 1985, 197-208.
[31] *Stress Intensity Factors*, China Academy of Aeronautics and Astronautics, Science Press, Beijing, 1993. (in Chinese)

ORCID iD

Cong Li https://orcid.org/0009-0005-6585-8280
Bin Hu https://orcid.org/0000-0002-5991-9551
Yan Meng https://orcid.org/0009-0004-3874-8927

How to cite this article: Li C., Hu B., Meng Y. Interactions between Defects and Imperfect Interfaces Analyzing by a Fast Multiple BEM, *J. Appl. Comput. Mech.*, xx(x), 2026, 1–11. https://doi.org/10.22055/jacm.2026.48782.5492